

Stability of parametrically driven, damped nonlinear Dirac solitonsBernardo Sánchez-Rey,¹ David Mellado-Alcedo,² and Niurka R. Quintero³

¹*Departamento de Física Aplicada I, Escuela Politécnica Superior,
Universidad de Sevilla, Virgen de África 7, 41011, Sevilla,
Spain*

²*Departamento de Matemática Aplicada I, ETSII, Universidad de Sevilla,
Avda Reina Mercedes s/n, 41012 Sevilla, Spain*

³*Departamento de Física Aplicada I, ETSII, Universidad de Sevilla,
Avda Reina Mercedes s/n, 41012 Sevilla, Spain^{a)}*

(*Electronic mail: niurka@us.es)

(*Electronic mail: dmellado@us.es)

(*Electronic mail: bernardo@us.es)

(Dated: 22 December 2025)

The linear stability of two exact stationary solutions of the parametrically driven, damped nonlinear Dirac equation is investigated. Stability is ascertained through the resolution of the eigenvalue problem, which stems from the linearization of this equation around the exact solutions. On the one hand, it is proven that one of these solutions is always unstable, which confirms previous analysis based on a variational method. On the other hand, it is shown that a sufficiently large dissipation guarantees the stability of the second solution. Specifically, we determine the stability curve that separates stable and unstable regions in the parameter space. The dependence of the stability diagram on the driven frequency is also studied, and it is shown that low-frequency solitons are stable across the entire parameter space. These results have been corroborated with extensive simulations of the parametrically driven and damped nonlinear Dirac equation by employing a novel and recently proposed numerical algorithm that minimizes discretization errors.

^{a)}Also at IMUS, University of Seville, Spain

The nonlinear Dirac equation has attracted a lot of attention in recent years. Far from being restricted to the realm of high-energy particle physics, it also describes nonlinear excitations in other fields, such as nonlinear optics and Bose-Einstein condensates. Since these kinds of systems are susceptible to being controlled and manipulated, they constitute an excellent benchmark to study relativistic solitons. Moreover, dissipative losses, present in all physical systems, cause a decay of the soliton amplitude. Therefore, an interesting question is whether a parametric force can inject energy from outside to compensate for the losses in such a way that the soliton becomes stable. In this paper, this question is answered affirmatively. In fact, we prove that one exact stationary soliton solution of the parametrically driven and damped nonlinear Dirac equation is linearly stable in the majority of the parameter space. Furthermore, it is shown that instability regions tend to disappear for sufficiently low frequencies.

I. INTRODUCTION

Exact analytical solutions of nonlinear systems are *rarae aves*. They are usually uncommon and difficult to find. In this respect, conservation laws are extremely useful tools to determine analytical solutions of nonlinear systems. From simple pendulum equation to the nonlinear Dirac equation (NLDE), oscillatory or stationary exact solutions can be derived by employing the conservation of energy, charge or momentum.¹⁻⁵ In addition to their intrinsic value, exact solutions are very helpful: first, since their stability can be rigorously investigated by linearizing perturbations around the exact solution, and solving the corresponding eigenvalue problem;⁶⁻⁸ and second, since they can be used as a basis to construct approximate solutions of perturbed nonlinear systems, for instance through the time-variation of collective coordinates,⁹⁻¹² by employing variational approaches,¹³ or via the method of moments.^{14,15}

One of these *rarae aves* is the soliton solution of the Gross-Neveu model.^{16,17} This solution is interesting not only in the context of high-energy physics, but also in other fields such as nonlinear waveguide arrays, where the NLDE has been found to describe their dynamics. This finding has triggered new and growing interest in the NLDE in recent years, particularly regarding the possibility of studying relativistic phenomena in accessible and controllable systems.¹⁸⁻²⁰ For instance, an optical analogue of the relativistic soliton was investigated in Ref.²¹. Nonlinear Dirac-like models have also been derived for Bose-Einstein condensates trapped in honeycomb optical

lattices²², where a variety of solitary wave solutions have been explored.^{23–27}

In Ref.²⁸, we extended the soliton solution of the Gross-Neveu model to the parametrically driven and damped nonlinear Dirac equation,

$$i\gamma^\mu \partial_\mu \Psi - \Psi + (\bar{\Psi}\Psi)\Psi = r e^{-i2\Omega t} \Psi^* - i\rho \gamma^0 \Psi. \quad (1)$$

Here, $\Psi(x, t)$ is a vector field with two spinor components, γ^0 and γ^1 are the 1+1 dimensional Dirac gamma matrices defined in Ref.²⁹, $\partial_\mu = \partial/\partial x^\mu$, where $x^0 = t$ and $x^1 = x$ are the temporal and spatial coordinates, respectively, $\bar{\Psi} = (\Psi^*)^T \gamma^0$ is the Dirac adjoint spinor, $\rho > 0$ is a dissipation coefficient, and $r e^{-i2\Omega t}$ is a complex time-dependent periodic parametric force, with amplitude $r > 0$, and frequency $2\Omega > 0$.

If the frequency of the spinor oscillations is locked to half of the external frequency, then the following two exact stationary solutions of Eq. (1) are obtained

$$\Psi_\pm(x, t) = e^{-i(\Omega t + \Theta_\pm/2)} \begin{bmatrix} \psi_\pm(x) \\ i\chi_\pm(x) \end{bmatrix}, \quad (2)$$

where the real phase Θ_\pm takes the values $\Theta_+ = \arcsin(\frac{\rho}{r})$ for the *positive* solution $\Psi_+(x, t)$, and $\Theta_- = \pi - \arcsin(\frac{\rho}{r})$ for the *negative* solution $\Psi_-(x, t)$. These conditions are identical to those for the stationary soliton solutions in the parametrically driven, damped nonlinear Schrödinger equation (NLSE).^{30,31} Similar requirements for the existence of nonlinear waves also arise in optical solitons with \mathcal{PT} -symmetric nonlinear couplers featuring gain and loss³² and in the parametrically driven and damped Ablowitz-Ladik equation.³³

In turn, the spatial part of the spinors is given by²⁸

$$\psi_\pm(x) = \sqrt{2}\beta_\pm \frac{\sqrt{1 + \omega_\pm} \cosh(\beta_\pm x)}{1 + \omega_\pm \cosh(2\beta_\pm x)}, \quad (3)$$

$$\chi_\pm(x) = \sqrt{2}\beta_\pm \frac{\sqrt{1 - \omega_\pm} \sinh(\beta_\pm x)}{1 + \omega_\pm \cosh(2\beta_\pm x)}, \quad (4)$$

where

$$\omega_\pm = \Omega + r \cos \Theta_\pm = \Omega \mp \sqrt{r^2 - \rho^2}, \quad (5)$$

$$\beta_\pm = \sqrt{1 - \omega_\pm^2}, \quad (6)$$

and $0 < \omega_\pm < 1$. As a consequence, for the *positive* solution to exist, it is necessary that $\rho < r < \sqrt{\rho^2 + \Omega^2}$, while, for the *negative* solution, $0 < \Omega < 1$ and $\rho < r < \sqrt{\rho^2 + (1 - \Omega)^2}$ must be fulfilled.

The introduction of a parametric force in the NLDE (1) was largely motivated by the study of parametric driving in the NLSE.^{30,34} The presence of dissipation attenuates nonlinear Schrödinger soliton speed and reduces its amplitude until its suppression. A key question therefore arises as to how to transfer energy into solitons to compensate for dissipative losses. Parametric driving results in an effective way to carry out said transfer and to stabilize damped nonlinear Schrödinger solitons.^{30,31,34–36} In the NLDE context, spatial periodic parametric forces were considered in Refs.^{37,38}, where the focus was on the length-scale competition between the soliton width and the spatial period of the force. Interestingly, when the damping term $-i\rho\gamma^0\Psi$ is introduced in this system, the soliton amplitude decays and eventually vanishes. Therefore, it is natural to pose the question regarding whether a temporal periodic parametric force can sustain damped solitons as in the NLSE. This means that the stability of the exact solutions (2) constitutes a crucial point of investigation. In Ref.²⁸, this issue was addressed by using a variational approach based on an ansatz with two collective coordinates. Similar to the study of the stability of the simple pendulum, the ansatz assumes a time-dependent frequency and a time-dependent phase that deviate slightly from the constant values ω_{\pm} and Θ_{\pm} , respectively. In this way, the soliton dynamics is reduced to a pair of coupled nonlinear ordinary differential equations. The advantage of this procedure is that soliton stability is mapped onto the stability analysis of two fixed points on a plane. In particular, it allows us to display phase portraits, where soliton dynamics is illustrated in a very intuitive way. Thus, for $\Omega = 0.5$, it was found that the solution $\Psi_+(x,t)$ was stable, whereas $\Psi_-(x,t)$ was unstable. Unfortunately, the method fails when exploring parameter space in more detail, especially regarding higher values of Ω .

For this reason, the aim of the current work is to rigorously investigate the stability of the stationary solutions $\Psi_{\pm}(x,t)$. In Section II, we consider an initial perturbation and linearize the parametrically driven, damped NLDE (1) around the exact solutions. After applying appropriate changes of variables,³⁰ the corresponding eigenvalue problem is obtained.^{39,40} Section III is devoted to numerically finding the eigenvalue spectrum by using a modified Chebyshev differentiation method.^{5,41} From said spectrum, a stability curve is derived that delineates the boundary between stable and unstable regions in parameter space for several values of the frequency Ω . These results are compared with direct numerical simulations of Eq. (1), taking $\Psi_{\pm}(x,0)$ as initial condition. For this task, Lakoba's method is employed, which is the most suitable for long-time and high-accuracy simulations.^{42–44} Both eigenvalue analysis and simulations confirm that $\Psi_-(x,t)$ is unstable. In contrast, the *positive* solution $\Psi_+(x,t)$ is stable in most of its existence domain,

except for tiny regions of very low dissipation. Strikingly, these unstable regions become smaller as the frequency Ω decreases. Lastly, our main conclusions are summarized in Section IV.

II. LINEAR STABILITY ANALYSIS

In order to study the stability of the exact stationary solutions (2), let us consider small perturbations $u(x, t)$ and $v(x, t)$ for the spinor components (3) and (4), such that we have the following perturbed solution

$$\Psi_{\pm}(x, t) = e^{-i[\Omega t + \Theta_{\pm}/2]} \begin{bmatrix} \psi_{\pm}(x) + u(x, t) \\ i\chi_{\pm}(x) + v(x, t) \end{bmatrix}. \quad (7)$$

For the sake of clarity, we will hereinafter omit the subscripts \pm in the functions $\psi_{\pm}(x)$, $\chi_{\pm}(x)$ and in parameters. By inserting (7) into the nonlinear Eq. (1) and linearizing with respect to the perturbations u and v , a system of two linear and coupled partial differential equations are obtained

$$\begin{aligned} i(u_t + v_x) - [1 - \Omega - \beta N(x)]u + [\psi^2(u + u^*) + i\chi\psi(v - v^*)] &= re^{i\Theta}u^* - i\rho u, \\ i(v_t + u_x) + [1 + \Omega - \beta N(x)]v - [i\chi\psi(u + u^*) - \chi^2(v - v^*)] &= -re^{i\Theta}v^* - i\rho v, \end{aligned} \quad (8)$$

where

$$N(x) = \frac{\psi^2(x) - \chi^2(x)}{\beta}.$$

Let us now introduce the variables $X = \beta x$ and $T = \beta t$. Since $u(x, t)$ and $v(x, t)$ are complex functions, it can be assumed, without loss of generality, that

$$u(X, T) = e^{-\tilde{\rho}T} [z_1(X, T) + iz_2(X, T)], \quad (9)$$

$$v(X, T) = e^{-\tilde{\rho}T} [z_3(X, T) + iz_4(X, T)], \quad (10)$$

where $\tilde{\rho} = \rho/\beta$. By substituting expressions (9)-(10) into Eqs. (8), it is straightforwardly obtained that the real and imaginary parts of $u(X, T)$ and $v(X, T)$ satisfy

$$z_{1T} - \tilde{\rho}z_1 = -z_{3X} - N(X)z_2 + \left(\frac{1}{\lambda} - \frac{1 + \lambda^2}{\lambda} \Omega \right) z_2, \quad (11)$$

$$z_{2T} + \tilde{\rho}z_2 = -z_{4X} + N(X)z_1 - \lambda z_1 + \frac{2}{\beta}(\psi^2 z_1 - \psi\chi z_4), \quad (12)$$

$$z_{3T} + \tilde{\rho}z_3 = -z_{1X} + N(X)z_4 - \frac{1}{\lambda}z_4 + \frac{2}{\beta}(\psi\chi z_1 - \chi^2 z_4), \quad (13)$$

$$z_{4T} - \tilde{\rho}z_4 = -z_{2X} - N(X)z_3 + \left(\lambda + \frac{1 + \lambda^2}{\lambda} \Omega \right) z_3, \quad (14)$$

where for the sake of simplicity, we have introduced the parameter

$$\lambda \equiv \lambda_{\pm} = \sqrt{\frac{1 - \omega_{\pm}}{1 + \omega_{\pm}}}, \quad 0 < \lambda < 1. \quad (15)$$

The advantage of this parametrization is that the two families of solutions are studied, as λ varies from 0 to 1. Specifically, the *negative* solution $\Psi_{-}(x, t)$ corresponds to the interval $0 < \lambda < \lambda_c$, where

$$\lambda_c = \sqrt{\frac{1 - \Omega}{1 + \Omega}}, \quad (16)$$

while we deal with the *positive* solution $\Psi_{+}(x, t)$, when $\lambda_c < \lambda < 1$.

The time and space dependence can now be separated by assuming

$$z_j(X, T) = \Re[\exp(\Gamma T)y_j(X)] = \exp(\Gamma_r T)\Re[\exp(i\Gamma_i T)y_j(X)], \quad j = 1, 2, 3, 4, \quad (17)$$

where $\Gamma = \Gamma_r + i\Gamma_i$, and $y_j(X)$ are complex functions that satisfy

$$(\Gamma - \tilde{\rho})y_1 = -y_{3X} - N(X)y_2 + \left(\frac{1}{\lambda} - \frac{1 + \lambda^2}{\lambda}\Omega\right)y_2, \quad (18)$$

$$(\Gamma + \tilde{\rho})y_2 = -y_{4X} + N(X)y_1 - \lambda y_1 + \frac{2}{\beta}(\psi^2 y_1 - \psi \chi y_4), \quad (19)$$

$$(\Gamma + \tilde{\rho})y_3 = -y_{1X} + N(X)y_4 - \frac{1}{\lambda}y_4 + \frac{2}{\beta}(\psi \chi y_1 - \chi^2 y_4), \quad (20)$$

$$(\Gamma - \tilde{\rho})y_4 = -y_{2X} - N(X)y_3 + \left(\lambda + \frac{1 + \lambda^2}{\lambda}\Omega\right)y_3. \quad (21)$$

A further change of variables $y_2(X) = \sqrt{(\Gamma - \tilde{\rho})/(\Gamma + \tilde{\rho})}\tilde{y}_2(X)$ and $y_3(X) = \sqrt{(\Gamma - \tilde{\rho})/(\Gamma + \tilde{\rho})}\tilde{y}_3(X)$ allows us to write the above system as an eigenvalue problem

$$\Lambda y_1 = -\tilde{y}_{3X} - \tilde{N}(X)\tilde{y}_2 + \left(\frac{1}{\lambda} - \frac{1 + \lambda^2}{\lambda}\Omega\right)\tilde{y}_2, \quad (22)$$

$$\Lambda \tilde{y}_2 = -y_{4X} + \tilde{N}(X)y_1 - \lambda y_1 + 2(\tilde{\psi}^2 y_1 - \tilde{\psi} \tilde{\chi} y_4), \quad (23)$$

$$\Lambda \tilde{y}_3 = -y_{1X} + \tilde{N}(X)y_4 - \frac{1}{\lambda}y_4 + 2(\tilde{\psi} \tilde{\chi} y_1 - \tilde{\chi}^2 y_4), \quad (24)$$

$$\Lambda y_4 = -\tilde{y}_{2X} - \tilde{N}(X)\tilde{y}_3 + \left(\lambda + \frac{1 + \lambda^2}{\lambda}\Omega\right)\tilde{y}_3, \quad (25)$$

where $\Lambda = \sqrt{\Gamma^2 - \tilde{\rho}^2}$, $\tilde{\psi}(X) = \psi(X)/\sqrt{\beta}$, $\tilde{\chi}(X) = \chi(X)/\sqrt{\beta}$, and $\tilde{N}(X) = \tilde{\psi}^2(X) - \tilde{\chi}^2(X)$.

In matrix form

$$\mathbf{M}\mathbf{y} = \Lambda\mathbf{y} \quad (26)$$

where $\mathbf{y} = (y_1, \tilde{y}_2, \tilde{y}_3, y_4)^T$, and the elements of \mathbf{M} are

$$\mathbf{M} = \begin{bmatrix} 0 & -\tilde{N}(X) + \frac{1}{\lambda} - \frac{1+\lambda^2}{\lambda}\Omega & -\frac{d}{dX} & 0 \\ \tilde{N}(X) + 2\tilde{\psi}^2 - \lambda & 0 & 0 & -\frac{d}{dX} - 2\tilde{\psi}\tilde{\chi} \\ -\frac{d}{dX} + 2\tilde{\psi}\tilde{\chi} & 0 & 0 & \tilde{N}(X) - 2\tilde{\chi}^2 - \frac{1}{\lambda} \\ 0 & -\frac{d}{dX} & -\tilde{N}(X) + \lambda + \frac{1+\lambda^2}{\lambda}\Omega & 0 \end{bmatrix}. \quad (27)$$

This system is invariant under the transformations $\{\Lambda, y_j(X)\} \rightarrow \{\Lambda^*, y_j^*(X)\}$ and $\{\Lambda, X, y_1, \tilde{y}_3\} \rightarrow \{-\Lambda, -X, -y_1, -\tilde{y}_3\}$. Consequently, if Λ is an eigenvalue, then Λ^* and $-\Lambda$ are also eigenvalues. Therefore, real or pure imaginary eigenvalues appear in pairs $\{-\Lambda, \Lambda\}$, while complex eigenvalues appear in quartets $\{-\Lambda, \Lambda, -\Lambda^*, \Lambda^*\}$. According to (9)-(10) and (17), the soliton solution will be unstable whenever $\Gamma_r > \tilde{\rho}$. In particular, if there exists any real eigenvalue Λ , then the soliton will be unstable.

Before solving (26) numerically, it is convenient to analyze the continuum spectrum. Far away from the soliton, when $X \rightarrow \pm\infty$, the system (26) reduces into a solvable linear problem

$$\mathbf{M}_l \mathbf{y} = \Lambda_l \mathbf{y} \quad (28)$$

where \mathbf{M}_l can be obtained by setting $\tilde{\psi}(X) = 0$ and $\tilde{\chi}(X) = 0$ in \mathbf{M} .

Seeking solutions of the form $y_j(X) = A_j e^{ikX}$, we found that $\Lambda_l = i\nu$, where

$$\nu^2(k) = 1 + k^2 + \frac{(1 + \lambda^2)\Omega}{2\lambda^2} \left[1 - \lambda^2 \pm \sqrt{(1 + \lambda^2)^2 + 4k^2\lambda^2} \right], \quad (29)$$

$\forall k \in \mathbb{R}$. Thus, the continuum spectrum is composed of two phonon bands. The upper band lies in the interval $[i\nu_2, +i\infty)$, where

$$\nu_2 = \sqrt{1 + \frac{(1 + \lambda^2)\Omega}{\lambda^2}}, \quad (30)$$

while the lower band is in the interval $[i\nu_1, +i\infty)$, with

$$\nu_1 = \sqrt{1 - \Omega(1 + \lambda^2)} < \nu_2. \quad (31)$$

Therefore, there is a gap in the spectrum between 0 and ν_1 . Furthermore, stability implies $1 - \Omega(1 + \lambda^2) > 0$, which entails $\lambda < \lambda_1 \equiv \sqrt{\frac{1-\Omega}{\Omega}}$.

III. NUMERICAL STUDY

In this section, we numerically solve the discretized version of the eigenvalue problem (26) in two steps. As a first step, by employing a modified Chebyshev differentiation method⁴⁵, (see

Appendix A for details), we discretize the spatial variable $X \in [-L, L]$ using the collocation points

$$X_n = 4 \operatorname{arctanh} \left[\cos \left(\frac{\pi n}{N+1} \right) \right], \quad n = 1, 2, \dots, N, \quad (32)$$

and solve the discretized equations for the spatial part of the spinors

$$\tilde{\psi}_{n,X} + \frac{1}{\lambda} \tilde{\chi}_n - (\tilde{\psi}_n^2 - \tilde{\chi}_n^2) \tilde{\chi}_n = 0, \quad (33)$$

$$\tilde{\chi}_{n,X} + \lambda \tilde{\psi}_n - (\tilde{\psi}_n^2 - \tilde{\chi}_n^2) \tilde{\psi}_n = 0, \quad (34)$$

where $\tilde{\psi}_n \equiv \tilde{\psi}(X_n)$, $\tilde{\chi}_n \equiv \tilde{\chi}(X_n)$, and the discrete derivatives $\tilde{\psi}_{n,X} \equiv \frac{d\tilde{\psi}}{dX}|_{X=X_n}$ and $\tilde{\chi}_{n,X} \equiv \frac{d\tilde{\chi}}{dX}|_{X=X_n}$ are computed by applying the Chebyshev differentiation operator. For this task, we employ the simplified Newton method⁴⁶ with the solution of the continuous system

$$\tilde{\psi}(X) = \frac{\sqrt{2\lambda} \cosh(X)}{\cosh^2(X) - \lambda^2 \sinh^2(X)}, \quad (35)$$

$$\tilde{\chi}(X) = \lambda \tanh(X) \tilde{\psi}(X), \quad (36)$$

as initial guess.

In a second step, we substitute the numerical solution of Eqs. (33)-(34) into the discrete version of the eigenvalue problem (26), and construct an $4N \times 4N$ matrix, again using the Chebyshev differentiation operator for the spatial derivative. The eigenvalue problem is then solved numerically.⁴⁷

Notice that for a fixed frequency Ω , the only parameter of the eigenvalue problem is λ , defined in Eq. (15). In addition the reduction in the number of free parameters, we recall that this parametrization has the advantage of allowing the two families of solutions to be studied as λ varies from 0 to 1.

A. The unstable stationary solution $\Psi_-(x, t)$

Let us start studying the stability of the stationary solution $\Psi_-(x, t)$ for which $0 < \lambda < \lambda_c$. As mentioned in the introduction, this solution exists whenever $0 < \Omega < 1$ and $\rho < r < \sqrt{\rho^2 + (1 - \Omega)^2}$. In this case, the eigenvalue spectrum of the stability matrix (27) shows real eigenvalues and, therefore, $\Psi_-(x, t)$ is unstable. This eigenvalue can clearly be observed in the top panel of Fig. 1 for $\Omega = 0.5$ (circles) and $\Omega = 0.9$ (squares). The instability grows faster as Ω decreases, and tends to zero when λ approaches λ_c , represented by the vertical dashed lines. Direct

simulations of Eq. (1) using Lakoba's method^{43,44} confirm this result. For $\Omega = 0.9$, $r = 0.08$, and $\rho = 0.025$ ($\lambda \simeq 0.11$), the initial condition $\Psi_-(x, 0)$ is unstable and evolves in time. The resulting charge density

$$\sigma(x, t) = \bar{\Psi}(x, t)\gamma^0\Psi(x, t) \quad (37)$$

have been represented in the middle panel of Fig. 1. As can be observed, at approximately $t = 100$, the *negative* solution evolves towards the *positive* solution $\Psi_+(x, t)$, which behaves as an attractor of the dynamics. This is confirmed in the bottom panel of Fig. 1, where it is shown that the charge densities $\sigma(x, 1000)$ and $\sigma_+(x) = \bar{\Psi}_+(x, t)\gamma^0\Psi_+(x, t)$, clearly overlap.

This phenomenon was already captured and well described by the collective coordinate approach in Ref.²⁸. We will verify in the next subsection that the *positive* solution is indeed stable for these parameter values.

B. The stability curve of the stationary solution $\Psi_+(x, t)$

Let us now investigate the stability of the solution $\Psi_+(x, t)$. This solution exists for $\rho \leq r < \sqrt{\rho^2 + \Omega^2}$, which, in terms of λ , implies that $\lambda_c < \lambda < 1$. For a given value of Ω , we have to study the eigenvalue spectrum while λ varies in that interval. From Section II, we know that the soliton will be stable if all eigenvalues are pure imaginary or, in the case that a complex quadruplet $\Lambda_q = \pm\Lambda_r \pm i\Lambda_i$ appears, if $\tilde{\rho} > \Gamma_r = \Lambda_r\Lambda_i/\sqrt{\Lambda_i^2 - \Lambda_r^2}$, ($\Lambda_i > \Lambda_r > 0$). Therefore, from the condition $\tilde{\rho} = \Gamma_r$, we can construct the curve $r(\rho)$ that separates the stable and unstable regions on the ρ - r plane. When, for a given λ , a complex quadruplet emerges, the coordinates of a point (ρ^*, r^*) on the separatrix are given by the dissipation coefficient

$$\rho^* = \beta\Gamma_r = \frac{2\lambda}{1+\lambda^2} \frac{\Lambda_r\Lambda_i}{\sqrt{\Lambda_i^2 - \Lambda_r^2}}, \quad (38)$$

and, taking (5) and (15) into account, by the amplitude of the parametric force

$$r^* = \sqrt{\rho^{*2} + (\Omega - \omega_+)^2} = \sqrt{\rho^{*2} + \left(\Omega - \frac{1 - \lambda^2}{1 + \lambda^2}\right)^2}. \quad (39)$$

1. Case $\Omega = 0.9$

As a first case, let us consider $\Omega = 0.9$. This choice implies $\lambda_c = \sqrt{0.1/1.9} \simeq 0.2294$ and $\lambda_1 = 1/3$. Therefore, the *positive* solution $\Psi_+(x, t)$ is unstable in the interval $1/3 < \lambda < 1$ due to phonon instabilities.

Stability of parametrically driven, damped nonlinear Dirac solitons

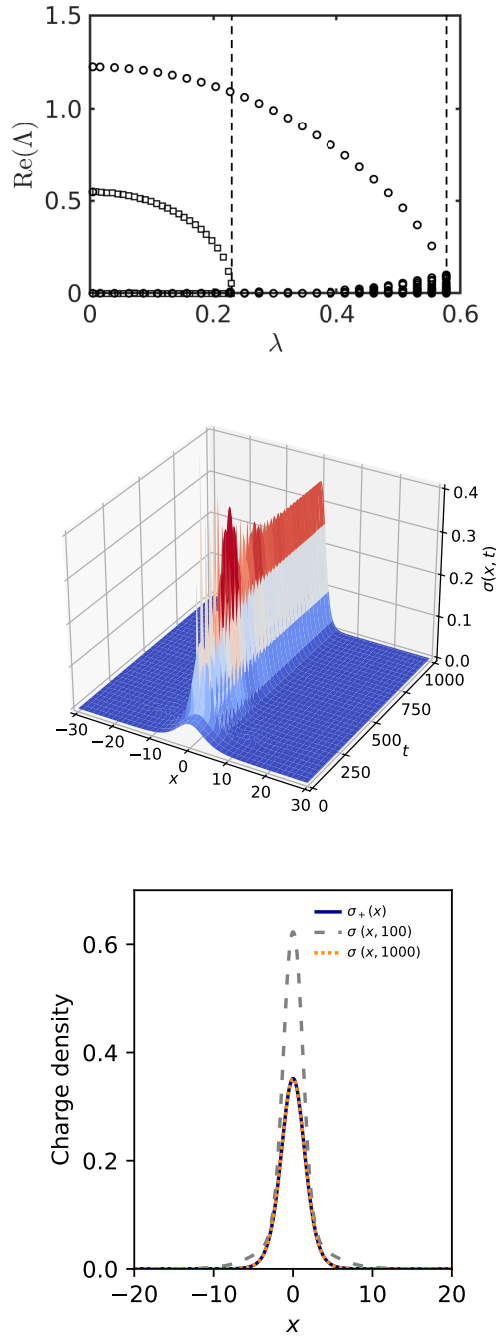


FIG. 1. Top panel: Real part of the eigenvalues of the stability matrix (27) for the stationary solution $\Psi_-(x,t)$ with $\Omega = 0.5$ (open circles) and $\Omega = 0.9$ (open squares). The dashed vertical lines represent the values of λ_c for both frequencies. The presence of a real eigenvalue implies that $\Psi_-(x,t)$ is unstable. Middle panel: Time evolution of $\sigma(x,0)$ for $\Omega = 0.9, r = 0.08$, and $\rho = 0.025$ ($\lambda \simeq 0.11$). The *negative* solution evolves towards the *positive* solution, which is an attractor of the dynamics. This is confirmed in the bottom panel, where we compare the charge densities $\sigma(x,100)$, $\sigma(x,1000)$ and $\sigma_+(x)$. In the simulation, we used a discretization step of $\Delta t = 0.01$ for time, and $\Delta x = 0.01$ for space.

As Fig. 2 shows, very near λ_c all eigenvalues are pure imaginary and the soliton is stable. As λ increases, one eigenvalue detaches from zero and moves upwards along the imaginary axis towards the lower edge of the phonon band. Subsequent to the collision, a complex quadruplet emerges approximately at $\lambda = 0.24$, and continues to exist as λ is subsequently increased.

With this quadruplet, we have employed the method described above, and have constructed the curve $r(\rho)$ that delineates the boundary between the stable and unstable regions on the ρ - r plane. This curve is plotted with a black dashed line in Fig. 3. This result has been corroborated by direct simulations of Eq. (1) using Lakoba's method, which is the most appropriate for the prevention of numerical instabilities due to discretization errors.⁴² In these simulations, we take the exact solution given by Eqs. (2) and (3)-(4), evaluated at $t = 0$, as the initial condition, and study its time evolution.

During the simulation, we track the soliton charge

$$Q(t) = \int_{-L}^L dx \bar{\Psi} \gamma^0 \Psi, \quad (40)$$

and its energy

$$E(t) = \int_{-L}^L dx \left[\frac{i}{2} \left(\bar{\Psi} \gamma^0 \Psi_t - \bar{\Psi}_t \gamma^0 \Psi \right) - \mathcal{L} \right], \quad (41)$$

where $L = 30$ is the system size, and $\mathcal{L} = \frac{i}{2} [\bar{\Psi} \gamma^\mu \partial_\mu \Psi - \partial_\mu \bar{\Psi} \gamma^\mu \Psi] - \bar{\Psi} \Psi + \frac{1}{2} (\bar{\Psi} \Psi)^2 - \frac{1}{2} f \bar{\Psi} \Psi^* - \frac{1}{2} f^* \bar{\Psi}^* \Psi$ is the lagrangian density, where $f(t) = r e^{-i2\Omega t}$ is the parametric force (see Ref.²⁸ for details). In order to verify the soliton stability, we compare $Q(t)$ and $E(t)$ with the charge and the energy of the exact solution

$$Q_+ = 2 \frac{\sqrt{1 - \omega_+^2}}{\omega_+}, \quad (42)$$

$$E_+ = 4 \operatorname{arctanh} \left(\sqrt{\frac{1 - \omega_+}{1 + \omega_+}} \right) + \sqrt{r^2 - \rho^2} Q_+. \quad (43)$$

More specifically, using a color code, the relative error of the charge

$$\varepsilon [Q(t)] = \frac{|Q(t) - Q_+|}{Q_+}, \quad (44)$$

evaluated at $t = 500$, is represented in the top panel of Fig. 3; while the relative error of the energy $\varepsilon [E(t)]$ is plotted in the bottom panel. These two relative errors are very similar, and show good agreement with the theoretical prediction for the location of the stable and unstable regions.

Stability of parametrically driven, damped nonlinear Dirac solitons

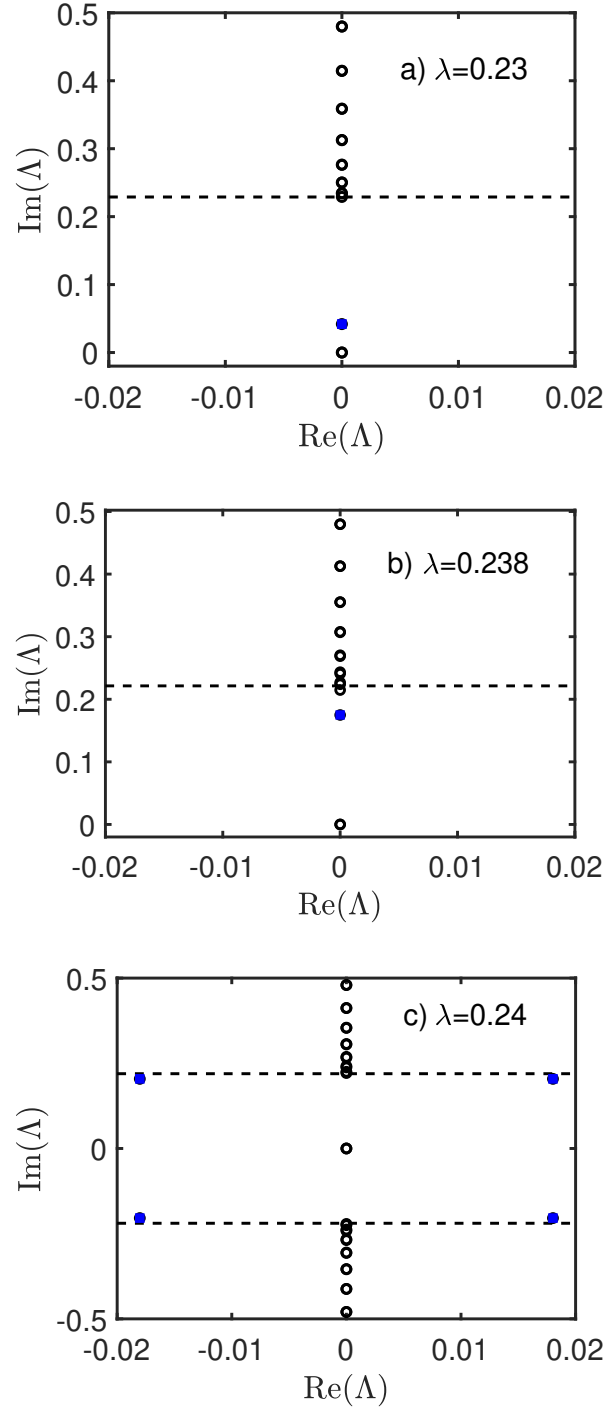


FIG. 2. Emergence of a complex quadruplet for $\Omega = 0.9$ as λ increases from $\lambda_c \simeq 0.2294$. The dashed line represents the lower border of the phonon band. Top panel: near λ_c all the eigenvalues are pure imaginary and the soliton is stable. Middle panel: as λ increases, an eigenvalue (filled circle) moves from zero upwards along the imaginary axis. Bottom panel: a complex quadruplet, depicted with filled circles, emerges when the eigenvalue coming from zero collides with a detached mode from the continuum. The spectrum of the matrix (27) has been computed using a Chebyshev grid of $N = 799$ points.

Our simulations confirm that, in the blue region, solitons remain stable even up to times $t = 10^4$. Therefore, the conclusion is that it is possible to stabilize solitons by adding sufficient dissipation.

Note also that the domain explored in the simulations is confined between the straight line $r_{min} = \rho$ (since there is no soliton solution for $r < \rho$), and the curve

$$r_{max} = \sqrt{\rho^2 + \left(\Omega - \frac{1 - \lambda_1^2}{1 + \lambda_1^2}\right)^2} = \sqrt{\rho^2 + (1 - \Omega)^2}, \quad (45)$$

because, for $\lambda > \lambda_1 = 1/3$, solitons are unstable with respect to the continuous spectrum.

2. Case $\Omega = 0.5$

A lower value of frequency is now fixed at $\Omega = 0.5$. For this value, $\lambda_c = \sqrt{1/3} \simeq 0.577$ and $\lambda_1 = 1$, and therefore the eigenvalue spectrum of the stability matrix must be studied in the interval $\sqrt{1/3} < \lambda < 1$. An intricate scenario arises due to the appearance of many bubbles around the imaginary axis, as can be observed in the left-hand panel of Fig. 4. Most of these bubbles are spurious, as has been described in the literature.^{48–50} The size of these bubbles decreases when the number of grid points, N , employed in the discretization of the matrix (27) are increased, that is, as the continuum limit is approached. It can also be verified that the associated eigenvectors show a staggered profile, which cannot be supported in the continuum limit. Furthermore, we have observed that changes in the domain size or in the number N cause changes in the location of the bubbles. As the continuum limit is approached, they are pushed away above the border v_2 of the upper phonon band (see the right-hand panel of Fig. 4). Although these observations guide us, it remains a highly cumbersome task to distinguish spurious bubbles from actual quadruplets that govern soliton stability.

In fact, direct simulations of the time evolution of $\Psi_+(x, 0)$ up to $t = 10000$ show that this soliton is stable in almost the entire parameter space (see Fig. 5). There appear only very small unstable lobes for very low dissipation. These unstable tiny regions were undetected with the collective coordinate method²⁸. Their borders agree well with the stability curve (white dashed line) that stems from the analysis of the spectrum, once all spurious bubbles have been discarded. The quadruplet responsible for the largest unstable lobe, that is, the intermediate red zone with a peak around $(0.007, 0.35)$, is displayed in the left-hand panel of Fig. 6. In the right-hand panel, the time evolution of $\sigma_+(x, 0)$ is presented for the parameter values $\rho = 0.002, r = 0.35$, corresponding

Stability of parametrically driven, damped nonlinear Dirac solitons

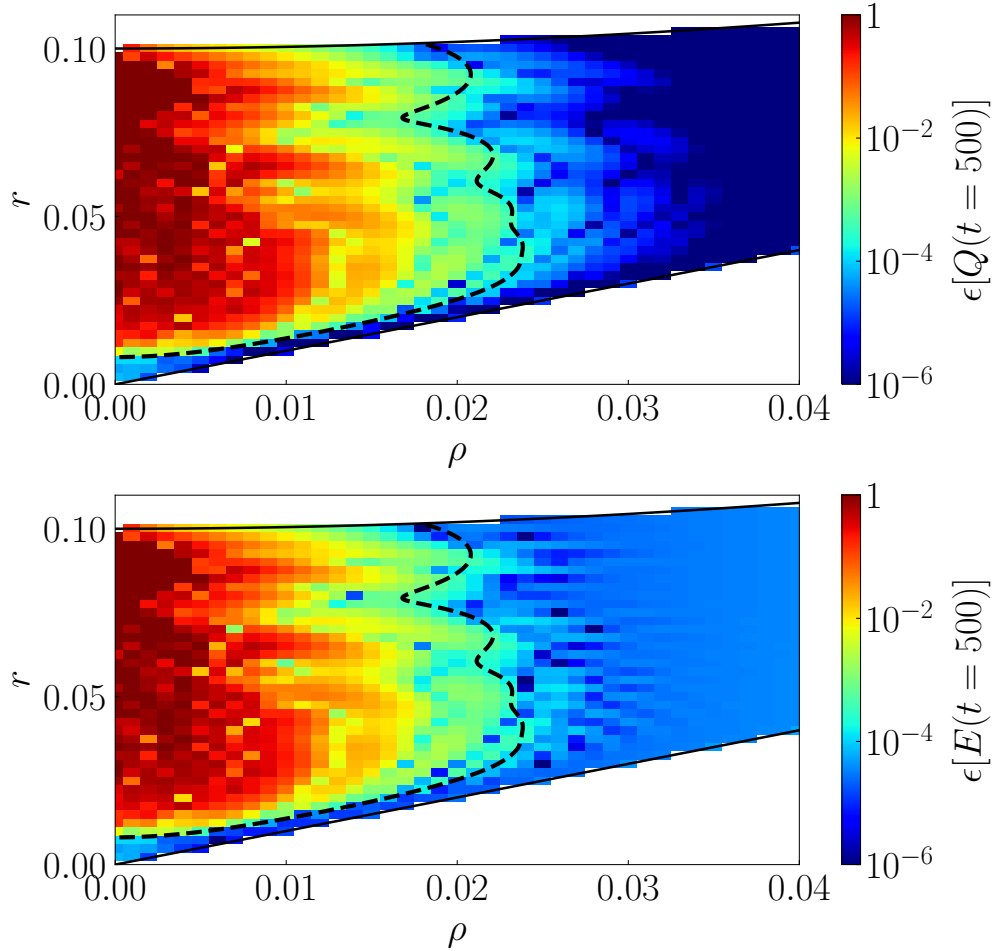


FIG. 3. Comparison between direct simulations of the NLDE (1), taking $\Psi_+(x,0)$ as initial condition, and the stability prediction that arises from the eigenvalue analysis for $\Omega = 0.9$. A color-coded representation is given of the relative error of the soliton charge (top panel) and the soliton energy (bottom panel) at $t = 500$. The black dashed line represents the stability curve, obtained from the eigenvalue analysis, which separates unstable and stable regions. In the lower white region below $r = \rho$ (straight black solid line) no soliton solutions exist. Above $r = \sqrt{\rho^2 + (1 - \Omega)^2}$ (upper black solid line), the soliton is unstable with respect to the continuum.

to a point located within the aforementioned red lobe. Notice that the soliton has two humps, whose apexes develop oscillations that grow over time.

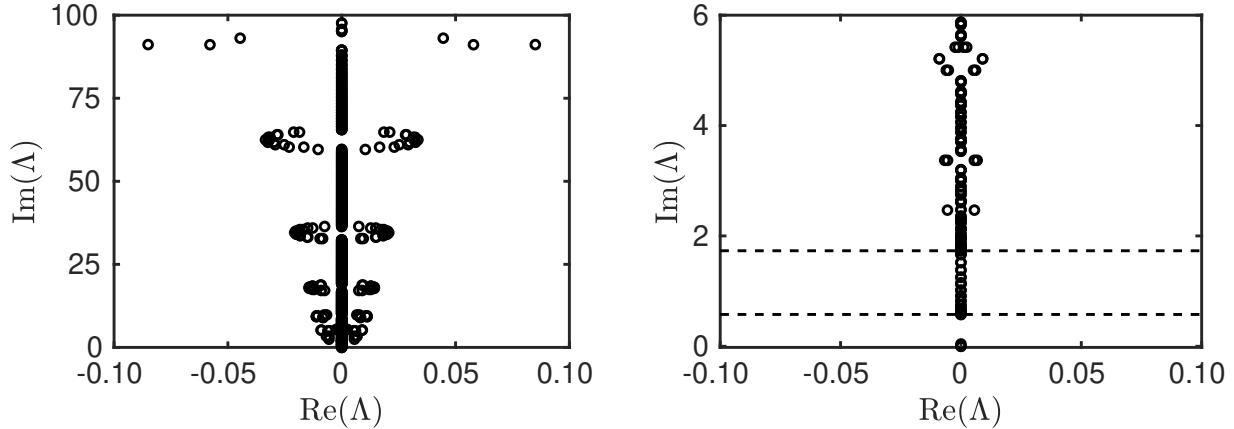


FIG. 4. Left-hand panel: Eigenvalue spectrum for $\Omega = 0.5$ and $\lambda = 0.578$, very near $\lambda_c \simeq 0.577$. Note the presence of numerous spurious bubbles around the imaginary axis. Right-hand panel: Zoom on the essential part of the spectrum. The dashed lines represent the borders, $v_1 \simeq 0.577$ and $v_2 \simeq 1.73$, of the lower and upper phonon bands, respectively.

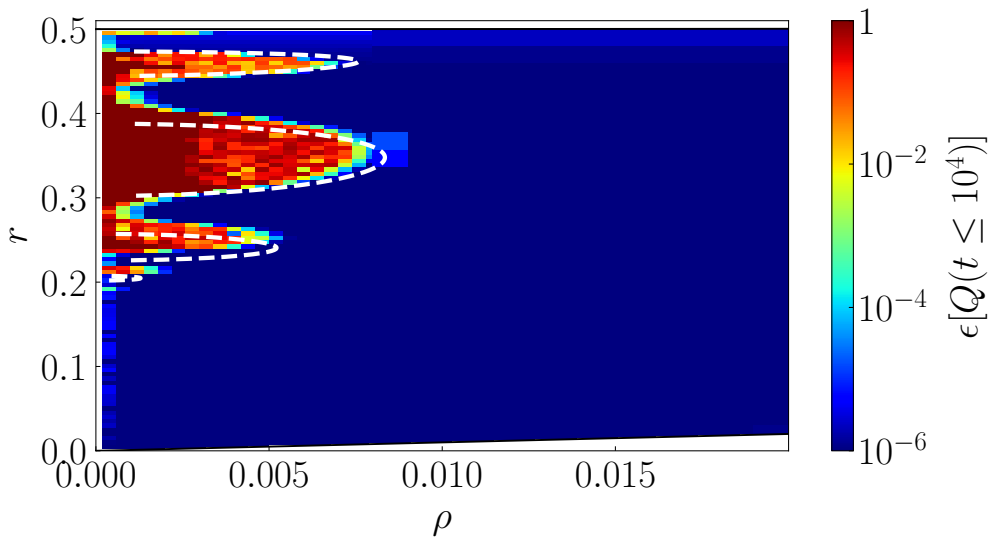


FIG. 5. Comparison between direct simulations of the NLDE (1), taking $\Psi_+(x, 0)$ as initial condition, and the stability prediction that arises from the eigenvalue analysis for $\Omega = 0.5$. A color-coded representation is given of the relative error of the soliton charge at $t = 10^4$. The white dashed line represents the stability curve, obtained from the eigenvalue analysis, which separates unstable and stable regions.

3. Case $\Omega = 0.2$

As a final case, $\Omega = 0.2$ is considered. Here, $\lambda_c \simeq 0.816$ and $\lambda_1 = 2$. Again, in the interval $\lambda_c < \lambda < 1$ many spurious bubbles arise but, surprisingly, no true instability is detected. The *positive*

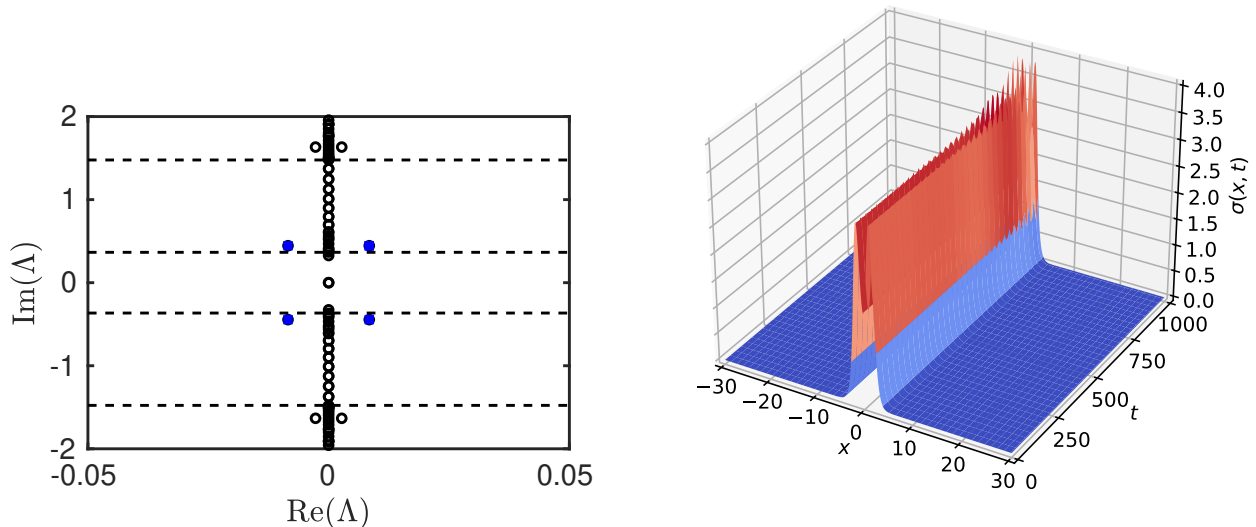


FIG. 6. Left-hand panel: The solid blue circles represent the quadruplet for $\lambda = 0.856$ ($\rho = 0.0064938$ and $r = 0.3458$), which is localized above v_1 and below $v_2 > v_1$, both represented with dashed lines. Right-hand panel: time evolution of $\sigma_+(x, 0)$ for $\Omega = 0.5$, $r = 0.35$, and $\rho = 0.002$. These parameter values lie in the unstable red region of Fig. 5. Note that the soliton has two humps and also the presence of increasing oscillations at the top of the humps.

solution is stable for all possible values of the parameters $0 < \rho < r$ and $0 < r < \sqrt{\rho^2 + \Omega^2}$, as corroborated by the simulation results shown in Fig. 7.

The progressive reduction of unstable areas in the parameter space when decreasing the frequency Ω is an unexpected result. It contrasts with the fact that the Gross-Neveu soliton becomes very sensitive to weak numerical instabilities as Ω decreases. In fact, in recent years, some controversy has existed regarding its stability for sufficiently small Ω .^{2,48,51,52} The debate was resolved by suggesting a numerical scheme based on the method of characteristics with absorbing boundary conditions, which prevents the interaction of the soliton with its own radiation emitted due to discretization errors.^{42,43,53} This interaction was precisely the cause of the instability observed. Although not a true instability, the sensitivity of low-frequency Gross-Neveu solitons to their own emitted radiation may be taken as an indicator of a lack of robustness. However, in the case of the parametrically driven and damped nonlinear Dirac solitons, low frequencies favor their stability.

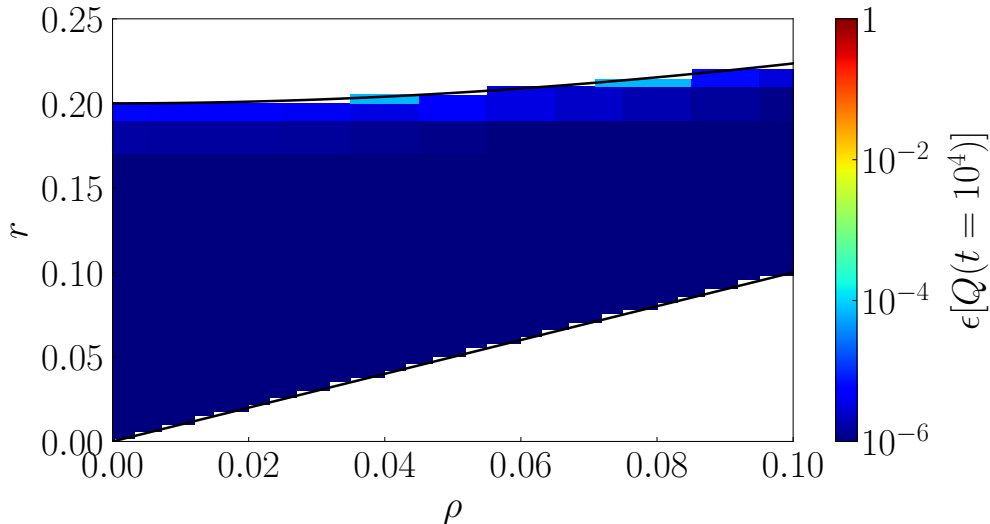


FIG. 7. Relative error of the soliton charge at $t = 10^4$ for $\Omega = 0.2$, obtained by direct simulations of the NLDE (1), taking $\Psi_+(x, 0)$ as initial condition. No instability is observed.

IV. CONCLUSIONS

We have investigated the linear stability of exact stationary soliton solutions of the parametrically driven and damped nonlinear Dirac equation. From the numerical resolution of the corresponding eigenvalue problem, we have obtained the stability curve that separates the stable and unstable regions in the parameter space. Our main result is that the *positive* solution, $\Psi_+(x, t)$, is stable in most of the parameter space, except for small domains of very low dissipation. In principle, damping causes an attenuation of the soliton amplitude, but we have proved that temporal periodic parametric driving can counterbalance the losses and stabilize the Dirac soliton, as was the case for the nonlinear Schrödinger soliton. Contrary to intuition, the larger dissipation, the easier it is to stabilize the soliton. We have also verified that in the stable region, $\Psi_+(x, t)$ behaves as an attractor of the dynamics such that the unstable negative solution $\Psi_-(x, t)$ evolves towards $\Psi_+(x, t)$.

We have explored several values of the frequency soliton Ω between 0 and 1. It should be borne in mind that the unstable zones in the parameter space become smaller as the frequency decreases. For low frequencies, many spurious bubbles appear in the eigenvalue spectrum that make the analysis overly intricate. However, direct numerical simulations of the NLDE, taking the exact soliton solution as initial condition, confirm the results of the stability analysis. Extensive simulations have been performed with Lakoba's method, which has been proven to minimize

discretization errors. The fact that instability regions in the parameter space reduce their size as the soliton frequency is decreased is a striking result, since it is well known that the robustness of the Gross-Neveu soliton rapidly diminishes with decreasing frequencies.

An open question remains regarding the existence of exact traveling soliton solutions in the parametrically driven, damped NLDE. Both the driving and the dissipation terms break the Lorentz invariance, and hence a moving soliton cannot be obtained simply by boosting a static soliton. Naturally, were they to exist, investigating their stability and whether stable moving solitons coexist with stable static solitons, or at least whether they are long-lived excitations, would be highly interesting to explore.

From a numerical perspective, a major challenge arises regarding the development of methods capable of suppressing or eliminating spurious eigenvalues in spectral analyses. These spurious eigenvalues obscure the true stability properties of the solutions, and necessitate independent verification through direct numerical simulations of the full equation.

ACKNOWLEDGMENTS

We thank Jesús Casado-Pascual and Nora V. Alexeeva for valuable discussion on this work. B.S-R. acknowledges support from Grant ProyExcel 0076 funded by Junta de Andalucías PAIDI 2020 program, and from Grant PID2021-122588NBI00 funded by the Spanish project MCIN/AEI/10.13039/501100011033. D.M-A. and N.R.Q. received support from FQM-415 (University of Seville, Spain).

Appendix A: Modified Chebyshev differentiation method

In this appendix, an outline is given of the numerical scheme employed to calculate the discrete derivatives of the spinors in order to construct the matrix (27).

Given a function $u(x)$, the Chebyshev differentiation method⁴⁷ first implements a numerical discretization $u(x) \rightarrow \mathbf{u} = \{u(x_j)\}$, by considering the collocation points $x_j = \cos[\pi j/(N+1)]$, $j = 0, 1, \dots, N+1$. The discrete spatial derivative is then obtained multiplying matrix \mathbf{D} by the

vector \mathbf{u} . The elements of the matrix are⁴¹

$$D_{00} = \frac{2N^2 + 1}{6} \quad (\text{A1})$$

$$D_{jj} = \frac{-x_j}{2(1-x_j^2)}, \quad j = 1, \dots, N \quad (\text{A2})$$

$$D_{N+1,N+1} = -D_{00} \quad (\text{A3})$$

$$D_{ij} = \frac{c_i(-1)^{i+j}}{c_j(x_i - x_j)}, \quad i \neq j \quad i, j = 0, \dots, N+1, \quad (\text{A4})$$

where $c_0 = c_{N+1} = 2$ and $c_i = 1, i = 1, \dots, N$.

Note that the Chebyshev grid covers the interval $[-1, 1]$. The change of variables $X_j = l \operatorname{arctanh}(x_j)$ ^{5,45}, where l is a real number, transforms the Chebyshev grid into the infinite domain $(-\infty, \infty)$. In our numerical computations $l = 4$ has been selected. Since our system is defined in the interval $X_j \in [-L, L]$, we set $L = l \operatorname{arctanh}\{\cos[\pi N/(N+1)]\}$ and discard the points $X_0 = -\infty$ and $X_{N+1} = \infty$. The elements of the modified $N \times N$ Chebyshev differentiation matrix $\tilde{\mathbf{D}}$ therefore reads:

$$\tilde{D}_{ij} = \frac{D_{ij}}{l \cosh^2(X_i/l)}, \quad i, j = 1, \dots, N. \quad (\text{A5})$$

Thus, the derivative $\frac{du(X)}{dX}$ evaluated at $X = X_i$ is computed as $\tilde{D}_{ij}u(X_j)$.

REFERENCES

- ¹R. Z. Sagdeev, D. A. Usikov, and G. M. Zaslavsky. *Nonlinear Physics: From the Pendulum to Turbulence and Chaos*. Contemporary concepts in physics. Harwood Academic Publishers, 1988.
- ²F. G. Mertens, N. R. Quintero, F. Cooper, A. Khare, and A. Saxena. Nonlinear Dirac equation solitary waves in external fields. *Phys. Rev. E*, 86:046602, 2012.
- ³E. N. Tsoy, I. M. Allayarov, and F. Kh. Abdullaev. Stable localized modes in asymmetric waveguides with gain and loss. *Opt. Lett.*, 39:4215, 2014.
- ⁴V. V. Konotop and D. A. Zezyulin. Families of stationary modes in complex potentials. *Opt. Lett.*, 39:5535, 2014.
- ⁵N. V. Alexeeva, I. V. Barashenkov, and A. Saxena. Spinor solitons and their \mathcal{PT} -symmetric offspring. *Ann. Phys.*, 403:198, 2019.
- ⁶D. J. Kaup. Perturbation theory for solitons in optical fibers. *Phys. Rev. A*, 42:5689, 1990.

- ⁷J. Yang. Complete eigenfunctions of linearized integrable equations expanded around a soliton solution. *J. Math. Phys.*, 41:6614, 2000.
- ⁸E. G. Charalampidis and S. I. Mistakidis. Two-component droplet phases and their spectral stability in one dimension. *Phys. Rev. A*, 111:013318, 2025.
- ⁹Y. Nogami, F. M. Toyama, and Z. Zhao. Nonlinear Dirac soliton in an external field. *J. Phys. A: Math. Gen.*, 28:1413, 1995.
- ¹⁰A. Sánchez and A. R. Bishop. Collective Coordinates and Length-Scale Competition in Spatially Inhomogeneous Soliton-Bearing Equations. *SIAM Rev*, 40:579, 1998.
- ¹¹B. Sánchez-Rey, J. Casado-Pascual, and N. R. Quintero. Kink ratchet induced by a time-dependent symmetric field potential. *Phys. Rev. E*, 94:012221, 2016.
- ¹²K. V. Yershov, V. P. Kravchuk, D. D. Sheka, O. V. Pylypovskyi, D. Makarov, and Yu. Gaididei. Geometry-induced motion of magnetic domain walls in curved nanostripes. *Phys. Rev. B*, 98:060409, 2018.
- ¹³B. Malomed. Variational methods in nonlinear fiber optics and related fields. *Prog. in Optics*, edited by E. Wolf, 43:71, North-Holland, Amsterdam, 2002.
- ¹⁴A. I. Maimistov. Evolution of solitary waves which are approximately solitons of a nonlinear Schrödinger equation. *Zh. Eksp. Teor. Fiz.*, 104:3620, 1993.
- ¹⁵N. R. Quintero, F. G. Mertens, and A. R. Bishop. Generalized traveling-wave method, variational approach, and modified conserved quantities for the perturbed nonlinear Schrödinger equation. *Phys. Rev. E*, 82:016606, 2010.
- ¹⁶D. J. Gross and A. Neveu. Dynamical symmetry breaking in asymptotically free field theories. *Phys. Rev. D*, 10:3235, 1974.
- ¹⁷S. Y. Lee, T. K. Kuo, and A. Gavrielides. Exact localized solutions of two-dimensional field theories of massive fermions with Fermi interactions. *Phys. Rev. D*, 12:2249, 1975.
- ¹⁸F. Dreisow, M. Heinrich, R. Keil, A. Tünnermann, S. Nolte, S. Longhi, and A. Szameit. Classical Simulation of Relativistic Zitterbewegung in Photonic Lattices. *Phys. Rev. Lett.*, 105:143902, 2010.
- ¹⁹S. Longhi. Classical simulation of relativistic quantum mechanics in periodic optical structures. *Appl. Phys. B*, 104:453, 2011.
- ²⁰J. M. Zeuner, N. K. Efremidis, R. Keil, F. Dreisow, D. N. Christodoulides, A. Tünnermann, S. Nolte, and A. Szameit. Optical analogues for massless Dirac particles and conical diffraction in one dimension. *Phys. Rev. Lett.*, 109:023602, 2012.

- ²¹T. X. Tran, S. Longhi, and F. Biancalana. Optical analogue of relativistic Dirac solitons in binary waveguide arrays. *Ann. Phys.*, 340:179, 2014.
- ²²L. H. Haddad and L. D. Carr. The nonlinear Dirac equation in Bose-Einstein condensates: Foundation and symmetries. *Phys. D: Nonlinear Phenom.*, 238:1413, 2009.
- ²³L. H. Haddad, C. M. Weaver, and L. D. Carr. The nonlinear Dirac equation in Bose-Einstein condensates: I. Relativistic solitons in armchair nanoribbon optical lattices. *New J. of Phys.*, 17:063033, 2015.
- ²⁴A. U. Khawaja. Exact localized and oscillatory solutions of the nonlinear spin and pseudospin symmetric Dirac equations. *Phys. Rev. A*, 90:052105, 2014.
- ²⁵E. Arévalo and L. Morales-Molina. Nonlinear excitations in the honeycomb lattice: Beyond the high-symmetry points of the band structure. *Phys. Rev. A*, 93:053816, 2016.
- ²⁶F. G. Mertens, F. Cooper, N. R. Quintero, S. Shao, A. Khare, and A. Saxena. Solitary waves in the nonlinear Dirac equation in the presence of external driving forces. *J. Phys A: Math. and Theor.*, 49:065402, 2016.
- ²⁷N. R. Quintero, S. Shao, R. Alvarez-Nodarse, and F. G. Mertens. Externally driven nonlinear Dirac equation revisited: theory and simulations. *J. Phys. A: Math. Theor.*, 52:155401, 2019.
- ²⁸N. R. Quintero and B. Sánchez-Rey. Exact stationary solutions of the parametrically driven and damped nonlinear Dirac equation. *Chaos*, 29:093129, 2019.
- ²⁹A. Alvarez and B. Carreras. Interaction dynamics for the solitary waves of a nonlinear Dirac model. *Phys. Lett. A*, 86:327, 1981.
- ³⁰I. V. Barashenkov, M. M. Bogdan, and V. I. Korobov. Stability Diagram of the Phase-Locked Solitons in the Parametrically Driven, Damped Nonlinear Schrödinger Equation. *Europhys. Lett.*, 15:113, 1991.
- ³¹I. V. Barashenkov, E. V. Zemlyanaya, and T. C. van Heerden. Time-periodic solitons in a damped-driven nonlinear Schrödinger equation. *Phys. Rev. E*, 83:056609, 2011.
- ³²N. V. Alexeeva, I. V. Barashenkov, A. A. Sukhorukov, and Yu. S. Kivshar. Optical solitons in \mathcal{PT} -symmetric nonlinear couplers with gain and loss. *Phys. Rev. A*, 85:063837, 2012.
- ³³J. Garnier, F. Kh. Abdullaev, and M. Salerno. Solitons in strongly driven discrete nonlinear Schrödinger-type models. *Phys. Rev. E*, 75:016615, 2007.
- ³⁴N. V. Alexeeva, I. V. Barashenkov, and D. E. Pelinovsky. Dynamics of the parametrically driven NLS solitons beyond the onset of the oscillatory instability. *Nonlinearity*, 12:103, 1999.
- ³⁵M. Bondila, I. V. Barashenkov, and M. M. Bogdan. Topography of attractors of the parametrically

- cally driven nonlinear Schrödinger equation. *Physica D*, 87:314, 1995.
- ³⁶F. Carreño-Navas, R. Alvarez-Nodarse, and N. R. Quintero. Oscillatory instability and stability of stationary solutions in the parametrically driven, damped nonlinear Schrödinger equation. *Phys. D: Nonlinear Phenom.*, 476:134611, 2025.
- ³⁷N. R. Quintero, B. Sánchez-Rey, F. Cooper, and F. G. Mertens. Length-scale competition in the parametrically driven nonlinear Dirac equation with a spatially periodic force. *J. Phys. A: Math. Theor.*, 52:285201, 2019.
- ³⁸F. Cooper, A. Khare, N. R. Quintero, B. Sánchez-Rey, F. G. Mertens, and A. Saxena. Parametrically driven nonlinear Dirac equation with arbitrary nonlinearity. *J. Phys. A: Math. Theor.*, 53:075203, 2020.
- ³⁹G. Berkolaiko and A. Comech. On Spectral Stability of Solitary Waves of Nonlinear Dirac Equation in 1D. *Math. Model. Nat. Phenom.*, 7:13, 2012.
- ⁴⁰J. Cuevas-Maraver, P. Kevrekidis, and A. Saxena. Solitary waves in a discrete nonlinear Dirac equation. *J. Phys. A: Math. Theor.*, 48:055204, 2015.
- ⁴¹M. Chugunova. *Spectral stability of nonlinear waves in dynamical systems*. Doctoral Thesis, McMaster University, Hamilton, Ontario, Canada, 2007.
- ⁴²T. I. Lakoba. Numerical study of solitary wave stability in cubic nonlinear Dirac equations in 1D. *Phys. Lett. A*, 382:300, 2018.
- ⁴³T. Lakoba and J. S. Jewell. Higher-order explicit schemes based on the method of characteristics for hyperbolic equations with crossing straight-line characteristics. *Numer. Methods Partial Differ. Equ.*, 37:2742, 2021.
- ⁴⁴D. Mellado-Alcedo and N. R. Quintero. Stability of nonlinear Dirac solitons under the action of external potential. *Chaos*, 34:013140, 2024.
- ⁴⁵M. Chugunova and D. Pelinovsky. Block-Diagonalization of the Symmetric First-Order Coupled-Mode System. *SIAM J. Appl. Dyn. Syst.*, 5:66, 2006.
- ⁴⁶J. M. Ortega and W. C. Rheinboldt. Chapter 7 - General Iterative Methods. In J. M. Ortega and W. C. Rheinboldt, editors, *Iterative Solution of Nonlinear Equations in Several Variables*, pages 181–239. Academic Press, 1970.
- ⁴⁷L. N. Trefethen. *Spectral methods in MATLAB*. SIAM, Philadelphia, 2000.
- ⁴⁸J. Cuevas-Maraver, P. Kevrekidis, A. Saxena, F. Cooper, and F. Mertens. *Ordinary and Partial Differential Equations*. Nova Sciences, New York, 2015.
- ⁴⁹D. Pelinovsky and Y. Shimabukuro. Transverse instability of line solitary waves in massive

Dirac equations. *J. Nonlinear Sci.*, 26:365, 2016.

⁵⁰I. V. Barashenkov and E. V. Zemlyanaya. Oscillatory instabilities of gap solitons: a numerical study. *Comput. Phys. Commun.*, 126:22, 2000.

⁵¹S. Shao, N. R. Quintero, F. G. Mertens, F. Cooper, A. Khare, and A. Saxena. Stability of solitary waves in the nonlinear Dirac equation with arbitrary nonlinearity. *Phys. Rev. E*, 90:032915, 2014.

⁵²A. Alvarez and B. Carreras. Energetic stability criterion for a nonlinear spinorial model. *Phys. Rev. Lett.*, 50:1230, 1983.

⁵³T. I. Lakoba. Study of instability of the Fourier split-step method for the massive Gross-Neveu model. *J. Comput. Phys.*, 402:109100, 2020.